Journal of Solid State Chemistry 181 (2008) 2350–2358

Contents lists available at ScienceDirect

Journal of Solid State Chemistry

journal homepage: www.elsevier.com/locate/jssc

Reactivity of metal oxides: Thermal and photochemical dissolution of *M*O and MFe_2O_4 (M = Ni, Co, Zn)

Luis A. García Rodenas [a,b], Miguel A. Blesa [a,c,d], Pedro J. Morando [a,b,c,*]

[a] Gerencia Química, Comisión Nacional de Energía Atómica, Centro Atómico Constituyentes, Avenida General Paz 1499, 1650 San Martín, Provincia de Buenos Aires, Argentina
[b] Instituto Jorge Sabato, Universidad Nacional de General San Martín, Argentina
[c] Consejo Nacional de Investigaciones Científicas y Técnicas (CONICET), Argentina
[d] Centro de Estudios Ambientales, Escuela de Posgrado, Universidad Nacional de General San Martín, Argentina

ARTICLE INFO

Article history:
Received 17 January 2008
Received in revised form
15 May 2008
Accepted 23 May 2008
Available online 29 May 2008

Keywords:
Co, Ni and Zn oxides
Co, Ni and Zn ferrites
Hematite
Me–O bond lability
Dissolution kinetics
Photodissolution
Water exchange

ABSTRACT

Dissolution rates of NiO, CoO, ZnO, α-Fe_2O_3 and the corresponding ferrites in 0.1 mol dm^{-3} oxalic acid at pH 3.5 were measured at 70 °C. The dissolution of simple oxides proceeds through the formation of surface metal oxalate complexes, followed by the transfer of surface complexes (rate-determining step). At constant pH, oxalate concentration and temperature, the trend in the first-order rate constant for the transfer of the surface complexes (k_{Me}; Me = Ni, Co, Zn, Fe) parallels that of water exchange in the dissolved metal ions (k_{-w}). Thus, the most important factor determining the rates of dissolution of metal oxides is the lability of Me–O bonds, which is in turn defined by the electronic structure of the metal ion and its charge/radius ratio. UV (384 nm) irradiation does not increase significantly the dissolution rates of NiO, CoO and ZnO, whereas hematite is highly sensitive to UV light. For ferrites, the reactivity order is $ZnFe_2O_4 > CoFe_2O_4 \gg NiFe_2O_4$. Dissolution is congruent, with rates intermediate between those of the constituent oxides, Fe_2O_3 and *M*O (M = Co, Ni, Zn), reflecting the behavior of very thin leached layers with little Zn and Co, but appreciable amounts of Ni. The more robust Ni^{2+} labilizes less the corresponding ferrite. The correlation between $\log k_M$ and $\log k_{-w}$ is somewhat blurred and displaced to lower k_M values. Fe(II), either photogenerated or added as salt, enhances the rate of Fe(III) phase transfer. A simple reaction mechanism is used to interpret the data.

1. Introduction

Dissolution of metal oxides in acidic aqueous solutions is, in principle, one of the simplest groups of heterogeneous inorganic reactions. Dissolution always involves protonation of oxo groups of the solid, rupture of Me–O bonds and phase transfer of the metal [1]. Often, the anions of the acid also play an important role, through surface complexation of metal ions, enhancement of proton co-adsorption, and labilization of vicinal Me–O bonds.

This group of reactions has been studied for very many years. Most of the studies focus on one particular aspect of the process: empirical rate laws to use in hydrometallurgy, influence of applied potential in the case of oxide electrodes, and morphological evolution of the metal oxide particles. Although a general picture has not been completely developed, it is now widely accepted that the inorganic chemistry of the interface governs the observed behavior; heterogeneous acid–base, complexation and electron transfer reactions are involved, and all of them bear important similarities with analogous homogeneous phenomena [1].

In spite of the many similarities between dissolved and surface metal ion chemistry, heterogeneous systems are more difficult to characterize because of the influence of the solid history. Trends in reactivity can be established by comparing the behavior of a given oxide in contact with a series of related reagents. Such studies, for instance, have established parallelisms between the stability of the surface and dissolved metal complexes [2,3]. A parallelism has also been established between the ligand-assisted mechanisms of metal detachment from a dissolving mineral surface and the mechanisms of ligand exchange around the corresponding metal ion in solution [4]. Similar ideas have been suggested to apply to the acid dissolution of NiO [5]. Here we show that, with adequate precautions, trends can also be established in the dissolution behavior of a series of related oxides in the presence of the same dissolution reagent. Often, the history of the solid produces quantitative changes in the observed kinetic behavior (rate constants), but the qualitative behavior (mechanism) remains unchanged.

In this paper we present a study of the thermal and photochemical dissolution of two oxides with rock-salt structure,

* Corresponding author at: Gerencia Química, Comisión Nacional de Energía Atómica, Centro Atómico Constituyentes, Avenida General Paz 1499, 1650 San Martín, Provincia de Buenos Aires, Argentina. Fax: +54 11 67727886.
E-mail address: morando@cnea.gov.ar (P.J. Morando).

0022-4596/$ - see front matter © 2008 Elsevier Inc. All rights reserved.
doi:10.1016/j.jssc.2008.05.032

CoO and NiO (bunsenite), and one with wurtzite structure, ZnO. All of them are highly soluble in mineral acids, but the rates of dissolution differ appreciably, the typical penetration rates at pH 1 ranging from 10^{-5} to 10^{-10} cm s^{-1} [1]. The chosen dissolution reagent was oxalic acid, which is known to be especially aggressive towards metal oxides, due to its combined properties of being a strong acid, a strong chelating agent and, under appropriate conditions, a good reductant [6]. Because of these properties, oxalic acid is an important constituent of many formulations used for chemical cleaning of metal surfaces. We also report data on α-Fe_2O_3. Although hematite has been much studied [7–9], the measurements were necessary because one of our objectives is to describe the dissolution of mixed oxides, namely ferrites of stoichiometry MFe_2O_4 (spinels with M = Co, Ni and Zn). Co and Ni ferrites are important constituents of the scales grown onto stainless steels. Furthermore, spinel ferrites constitute an important group of materials with many uses, and they are often synthesized from aqueous media by soft preparative procedures. Hence, the reverse dissolution reaction is important not only because of the corrosion processes the materials may undergo in wet atmospheres, but also in order to understand the nature of the interface ferrite/water in synthetic procedures. As described below, the nature of the surface in contact with aqueous solutions may differ appreciably from bulk composition. We found previously [10] that, in general, the rate of dissolution is intermediate, higher than that of the more robust constituent metal oxide, and lower than that of the more labile one. Frequently, after incongruent dissolution of a small fraction of the solid, the stoichiometry of dissolution becomes congruent, and both metal ions are transferred at the same rate.

Understanding of the factors that govern the dissolution of mixed metal oxides is limited by the need to distinguish between 'intrinsic' (structural chemistry) and 'extrinsic' factors (particle size, morphology and history). We have attempted to minimize extrinsic factors by controlling the preparative procedures, in order to focus on the response of each constituent to the medium conditions. Chemical parameters may affect the rates of dissolution of the component oxides in opposite ways. For example, Fe(III) oxides' dissolution rates are enhanced by the presence of reductants, whereas all M(II) oxides involved in the studied ferrites dissolve faster in the presence of oxidants. Thus, in this paper the influence of O_2 and Fe^{2+} is studied.

The effect of light on the rate of dissolution of metal oxides has been explored by several groups [11–15]. Again, similarities are found between the photochemistry of dissolved and surface metal complexes; this interaction with light may or may not produce dissolution rate enhancement.

Photochemical dissolution starts always through the absorption of a photon by the solid. With UV light ($\lambda = 384$ nm), the main primary photophysical event is the generation of an electron–hole pair. Direct absorption by surface chromophores (oxalato complexes) is also possible, but the effective absorption cross-section is comparatively small. The semiconducting properties of the oxides are therefore relevant. Both CoO and NiO are p-type [16] wide band semiconductors, whereas ZnO [1] and α-Fe_2O_3 are n-type [17]. Our final goal is to establish relationships between the kinetic properties of the dissolved ions and the rates of dissolution.

In the case of ferrites, the different response to light of both constituent oxides makes difficult the prediction of the effect of irradiation on dissolution kinetics; the results of the present study permit to integrate the mechanism of photochemical dissolution with the mechanism of thermal dissolution.

2. Materials and methods

2.1. Synthesis and characterization of the solid

Nearly stoichiometric spherical particles of NiO, ZnO and ferrites of narrow size distribution were prepared using a modified procedure based on Tamura and Matijević's method [18]. For NiO, ZnO and ferrites, KOH (0.08 mol) was added to a cylindrical reaction vessel containing 750 cm^3 of double-distilled water, and in the case of ferrites KNO_3 (0.16 mol) was also added. N_2 was bubbled through the solution for 2 h. For pure oxides, 50 cm^3 of a solution containing 0.04 mol of $M(NO_3)_2$ (M = Ni and Zn) was poured into the vessel. For mixed oxides, the solution contains $FeSO_4$ and $M(NO_3)_2$ (M = Ni, Co, Zn); the total amount of metal ions was kept constant at 0.04 mol, with a molar ratio [M]:[Fe] = 0.5. The reaction vessel containing $M(OH)_2$ (pure oxides) or the coprecipitated $Fe(OH)_2$ and $M(OH)_2$ (mixed oxides) was immersed in a bath at 90 °C, and the solids were aged for 4 h with continuous stirring and N_2 purge.

The solids were filtered through Millipore membranes (0.45 μm pore size) and heated for 1 h at 700 °C and then cooled to room temperature in an air atmosphere.

Attempts to prepare CoO always yielded a solid containing variable amounts of Co_3O_4. Therefore, a commercial sample was used (Merck, 99.99% purity).

Hematite was prepared by transformation of ferrihydrite [19]. In all, 40 g $Fe(NO_3)_3 \cdot 9H_2O$ was dissolved in 500 cm^3 twice distilled water preheated at 90 °C and ferrihydrite was precipitated with 300 cm^3 1 M KOH preheated at 90 °C. Then 50 cm^3 1 M $NaHCO_3$ was added, preheated to 90 °C and the suspension was kept (pH = 8–9) in a closed polyethylene flask at 90 °C for 48 h.

Metal content was measured by ICP optical emission spectrometry in a Perkin-Elmer Optima 3100 ICO-OES spectrometer AS 90 autosampler with conical vials or by atomic absorption spectrometry in a Perkin-Elmer A Analyst 100 apparatus. Iron content in the case of ferrites was measured spectrophotometrically using mercaptoacetic acid [20] in a Shimadzu UV-210A spectrophotometer. Particle morphology and size were characterized by scanning electron microscopy (SEM) using a Phillips SEM 500 apparatus, and near-surface composition was determined by EDS. Specific surface area (BET method) measurements were obtained in a Micromeritics AccuSorb 2100 E equipment and diffraction patterns were recorded in a Siemens D5000 diffractometer equipped with a graphite monochromator, and Cu$K\alpha$ radiation. The diffractograms of NiO [21], CoO [22], ZnO [23] and Fe_2O_3 [24] showed sharp peaks at the expected spacings.

The existence of a small fraction of hematite in cobalt and nickel ferrites was demonstrated by X-ray diffraction and EDS. Hematite is present as a thin surface layer; the hematite diffraction peaks disappear when ca. 12% of the solid is dissolved with oxalic acid and the diffractograms show only the sharp peaks of $NiFe_2O_4$ [25], $CoFe_2O_4$ [26] and $ZnFe_2O_4$ [27]. All the experiments were carried out with these pickled samples.

Table 1 summarizes the bulk composition (average of three determinations) and the main characteristics of the synthesized oxides.

SEM pictures of ferrites show spherical particles with average diameters in the order of 0.1, 0.2, and 0.3 μm for M = Zn, Ni, and Co ferrites, respectively.

2.2. Kinetic experiments

Thermal kinetic experiments were performed in the dark under N_2 or O_2 atmosphere, in a magnetically stirred vessel immersed in a thermostat at 70.0 ± 0.1 °C. The oxide (ca. 20 mg)

Table 1
Characteristics of the synthesized oxides

Oxide	Semiconduction type	Composition	Surface area ($m^2 g^{-1}$)	Average particle diameter (μm)
NiO	p	$Ni_{1.04}O$	45.1	0.02
CoO	p	$Co_{0.98}O$	0.79	1.2
ZnO	n	$Zn_{1.02}O$	4.12	0.3
Fe_2O_3	n	$Fe_{2.03}O_3$	8.72	0.1
$NiFe_2O_4$	p	$Ni_{1.15}Fe_{1.90}O_4$	10.3	0.2
$CoFe_2O_4$	n	$Co_{1.00}Fe_{2.00}O_4$	3.9	0.3
$ZnFe_2O_4$	n	$Zn_{0.88}Fe_{2.08}O_4$	31.2	0.1

was poured over 100 cm^3 0.1 M oxalic acid solution; ionic strength was fixed at 0.5 M with $NaClO_4$ and pH was set at 3.5 with NaOH. At adequate time intervals, 1 cm^3 samples were taken and filtered through a 0.45-μm cellulose acetate membrane. Metal ions in the filtrate were measured as described before. In experiments designed to probe the influence of ferrous salts, adequate amounts of $Fe(NH_4)_2(SO_4)_2$ were added to the initial solution.

Photodissolution experiments were carried out in a reaction vessel illuminated from above with a 1000-W xenon lamp through an interference filter centered at 384 nm. Incident light intensity per unit solution volume was determined by chemical actinometry with trisoxalatoferrate(III), $I_o = 9.4 \times 10^{-6}$ einstein $s^{-1}\,dm^{-3}$.

3. Results

3.1. Thermal dissolution

In large excess oxalic acid, the stoichiometry of the thermal dissolution for the *M*O oxides is given by Eq. (1), whereas for hematite Eq. (2) applies. Metal oxide solubility is in principle high enough to guarantee total dissolution at pH 3.5. However, *M*(II) oxalates are sparingly soluble, and they may precipitate. This is indeed the case of Co(II) that reaches a maximum dissolution fraction ($f = [M]/[M]_T$, where $[M]_T$ is the expected concentration for total dissolution) of 0.4 in the dark and 0.6 under light:

$$MO(s) + 2HC_2O_4^- \rightarrow M(C_2O_4)_2^{2-} + H_2O \quad (1)$$

$$Fe_2O_3(s) + 6HC_2O_4^- \rightarrow 2Fe(C_2O_4)_3^{3-} + 3H_2O \quad (2)$$

The stoichiometry of dissolution for the ferrites is shown in Eq. (3). The thermal redox decomposition of 1.7×10^{-4} mol dm^{-3} trisoxalatoferrate(III) yields less than 5% Fe(II) at 70 °C and therefore does not affect appreciably the dissolution stoichiometry:

$$MFe_2O_4(s) + (6+n)HC_2O_4^- + (2-n)H^+ \rightarrow M(C_2O_4)_n^{(2n-2)-} + 2Fe(C_2O_4)_3^{3-} + 4H_2O \quad (3)$$

Fig. 1 shows the time evolution of the dissolution fractions for NiO, ZnO, α-Fe_2O_3 and CoO as a function of time. The maximum dissolution fraction of CoO is smaller than NiO and ZnO; probably coating of the particles by CoC_2O_4 produces passivity.

Fig. 2 shows the dissolved fraction f_{Me}/time profiles ($f_{Me} = [Me]/[Me]_T$, with *Me* = M or Fe; $[Me]_T$ is the expected concentration for total dissolution) for both metals in cobalt ferrite. Dissolution is congruent ($f_{Fe} = f_{Co}$) within the time span of our experiments and proceeds at a constant specific dissolution rate *k* (mol $m^{-2}\,s^{-1}$). Nickel and zinc ferrites follow the same congruent behavior (not shown).

In all pure and mixed oxides the thermal profiles are deceleratory and can be fitted by a simple contracting volume rate law (Eq. (4), where *k*′ is the specific dissolution rate constant

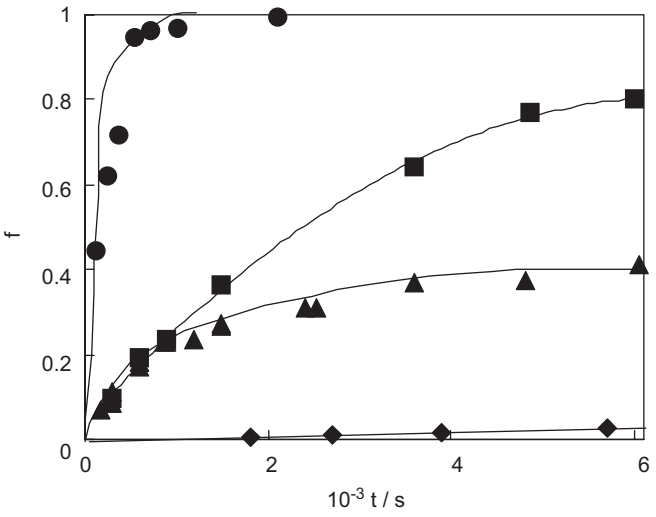

Fig. 1. Thermal dissolution profiles for NiO (■), CoO (▲), ZnO (●) and Fe_2O_3 (◆) in 0.1 M oxalic acid at 70 °C and pH 3.5 ($I = 0.5$ M $NaClO_4$).

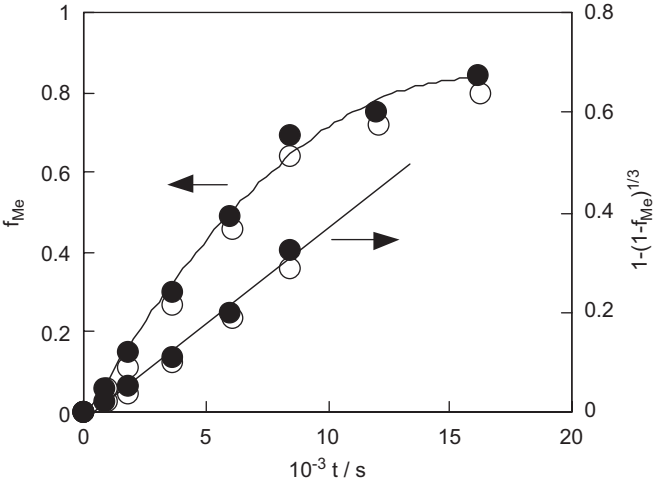

Fig. 2. *Upper curve*: time evolution of the Co (●) and Fe (○) thermal dissolution fractions ($f = [Me]/[Me]_T$) for $CoFe_2O_4$. *Lower line*: linear contracting volume expression (Eq. [4]) for Co (●) and Fe (○) dissolution. Experimental conditions: 0.1 M oxalic acid at 70 °C and pH 3.5 ($I = 0.5$ M $NaClO_4$).

(s^{-1})) up to appreciable degrees of conversion. This law implies constant reactivity per unit area, approximation valid for rather large particles with appreciable kinetic robustness. Fitting to this kinetic law is limited essentially by the formation of insoluble Co or Ni oxalates that arrests dissolution (see Fig. 1). The formation of insoluble oxalates is not important in the case of ferrites. In pure oxides of general formula M_xO, the specific dissolution rate *k* (mol $m^{-2}\,s^{-1}$) relates to *k*′ through Eq. (5), where S^0 is the initial

value of the specific surface area S, M_w is the oxide molecular weight and x is the metal stoichiometric coefficient in the oxide M_xO (x deviates from unity as indicated in Table 1). This regime implies that the penetration rate p ($cm\,s^{-1}$) usually defined as $p = -dr/dt$ (where r is the particle radius) is also constant and proportional to k and k' [1]:

$$1-(1-f)^{1/3} = k't \tag{4}$$

$$k = 3xk'/S^0M_w \tag{5}$$

In ferrites of general formula $M_{1-y}Fe_{2+x}O_4$ ($y = (3/2)x$), the specific dissolution rate k relates to k' through Eq. (6). The specific rates of dissolution of each individual ion Fe and M are, respectively, $k_{Fe} = \{(2+x)k\}$ and $k_M = \{(1-y)k\}$:

$$k = 3k'/S^0M_w \tag{6}$$

Fig. 2 includes the fitting of the data according to the integrated contracting volume rate law for both ions of $CoFe_2O_4$, Eq. (4).

Table 2 shows the k_{Me} values for pure and mixed oxides; the reactivity order in both cases is Zn > Co ≫ Ni.

Addition of ferrous ions increases the rates of dissolution of nickel and cobalt ferrites, without changing significantly that of zinc ferrite. Fig. 3 shows the specific rate enhancement R, as a function of $[Fe^{2+}]_0$. R is defined as $k_M^{Fe(II)}/k_M$, where $k_M^{Fe(II)}$ is the specific rate at any given value of $[Fe^{2+}]_0$, and k_M is the rate in the absence of Fe^{2+} (from Table 2). At high $[Fe^{2+}]_0$, a constant maximum rate is achieved ($k_{M\,max}^{Fe(II)}$).

Table 2
Thermal specific dissolution rates k_{Me} ($mol\,m^{-2}\,s^{-1}$) for the oxides in 0.1 M oxalic acid at 70 °C and pH 3.5

Oxide	$10^7 \times k_{Me}$ ($mol\,m^{-2}\,s^{-1}$)
$Ni_{1.04}O$	0.667
$Co_{0.98}O$	65.4
$Zn_{1.02}O$	98.4
$Fe_{2.03}O_3$	0.069
$Ni_{1.15}Fe_{1.90}O_4$	0.036[a]
$Co_{1.00}Fe_{2.00}O_4$	1.10[a]
$Zn_{0.88}Fe_{2.08}O_4$	1.74[a]

[a] Me = M(II).

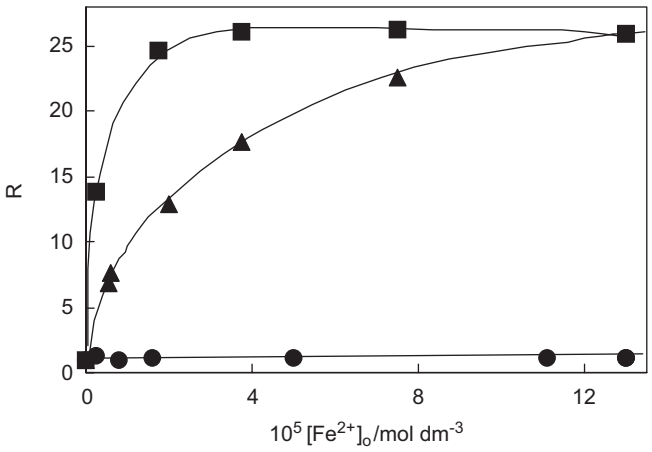

Fig. 3. Dependence on $[Fe^{2+}]_o$ of the acceleration factor $R = k_M^{Fe(II)}/k_M$ for the specific dissolution rate of $NiFe_2O_4$ (■), $CoFe_2O_4$ (▲) and $ZnFe_2O_4$ (●). Experimental conditions: 0.1 M oxalic acid at 70 °C and pH 3.5 (I = 0.5 M $NaClO_4$).

The shapes of the curves for Ni and Co ferrites can be described by Langmuir–Hinshelwood Eq. (7), where $R^{max} = k_{M\,max}^{Fe(II)}/k_M$ is the maximum acceleration factor and K_L the binding constant of Fe(II) on the surface (mediated by oxalate). Table 3 shows the values of $k_{M\,max}^{Fe(II)}$, K_L and R^{max} for nickel and cobalt ferrites. For zinc ferrite, if Eq. (7) applies, $R^{max} \cong 1$ and/or $K_L \cong 0$. The order of reactivity at high ferrous concentrations ($k_{M\,max}^{Fe(II)}$) is $CoFe_2O_4 \gg ZnFe_2O_4 > NiFe_2O_4$. The maximum acceleration factors are similar for nickel and cobalt ferrites, but in the second case higher concentrations of Fe^{2+} are required to achieve this factor because K_L is lower:

$$R = \frac{R^{max}K_L[Fe(II)]}{1+K_L[Fe(II)]} \tag{7}$$

Fig. 4 shows that the dissolved oxygen does not affect significantly the rate of dissolution of cobalt ferrite, except perhaps at high conversions, where dissolution is somewhat arrested; on the other hand, nickel ferrite dissolution rate is significantly enhanced. The profile for zinc ferrite dissolution, not shown, is not affected by oxygen.

Oxygen quenches the effect of Fe(II) addition, because the oxidation to Fe(III) is very fast. Sub-stoichiometric amounts of oxygen simply change the concentration of Fe(II) (see Fig. 3). Under excess oxygen, Fig. 4 applies.

3.2. Photochemical dissolution

Fig. 5 shows the time evolution of the dissolution fractions under illumination for the simple oxides. The results demonstrate a negligible influence of light for Ni and Zn oxides (see Fig. 1). In the CoO case, the dissolution fraction increases under light; coating of the particles by CoC_2O_4 probably produces passivity as it was observed in the dark dissolution. The photochemical dissolution profile for α-Fe_2O_3 is sigmoidal, and the simple contracting volume rate law does not apply.

The stoichiometry of hematite photodissolution is given by Eq. (8), whereas that of MO dissolution does not change under light (Eq. (1)):

$$Fe_2O_3(s) + HC_2O_4^- + 5H^+ \rightarrow 2Fe^{2+} + 2CO_2 + 3H_2O \tag{8}$$

In homogeneous solution, photochemical decomposition of trisoxalatoferrate(III) takes place with a quantum yield of 1.2 [28]. Under the experimental conditions used in this study, the photonic flux suffices to reduce all Fe^{3+} in 10 s and the stoichiometry of the photodissolution of ferrites is now given by Eq. (9). In Eqs. (8) and (9) complexation of dissolved ions has been ignored for simplicity:

$$MFe_2O_4(s) + HC_2O_4^- + 7H^+ \rightarrow M^{2+} + 2Fe^{2+} + 2CO_2 + 4H_2O \tag{9}$$

Irradiation with $\lambda_{max} = 384$ nm ($I_o = 9.4 \times 10^{-6}$ einstein s^{-1} dm^{-3}) brings about kinetic changes that parallel those produced by ferrous ion.

Table 4 shows the values of the photochemical dissolution rate (${}^{ph}k_M$) for oxides and the rate enhancement factors $R' = {}^{ph}k_M/k_M$, where k_M is the thermal dissolution rate (from Table 2). The results demonstrate a negligible influence of light for Ni and Zn oxides, and a little influence for Co oxides. For Ni and Co ferrites there is an appreciable influence of light and the order of reactivity is $CoFe_2O_4 > ZnFe_2O_4 > NiFe_2O_4$.

Even though the data in Table 4 are casted in terms of the same kinetic law as found for thermal dissolution, cobalt ferrite photodissolution rate at short times is lower than expected. Fig. 6 shows that a slightly sigmoidal profile is observed, similar to those measured earlier in the dissolution of magnetite [29] and in the

Table 3
Langmuir–Hinshelwood parameters for the dissolution of ferrites in 0.1 M oxalic acid at 70 °C and pH 3.5 in the presence of ferrous salts and rate enhancement factor R^{max}

Ferrite	$10^7 \times k_{M\,max}^{Fe(II)}$ (mol m^{-2} s^{-1})	$10^{-4} \times K_L$ ((mol Fe^{2+})$^{-1}$ dm^3)	$R^{max} = k_{M\,max}^{Fe(II)}/k_M$
$Ni_{1.15}Fe_{1.90}O_4$	0.96	39.4	26.7
$Co_{1.00}Fe_{2.00}O_4$	26.63	7.26	24.2

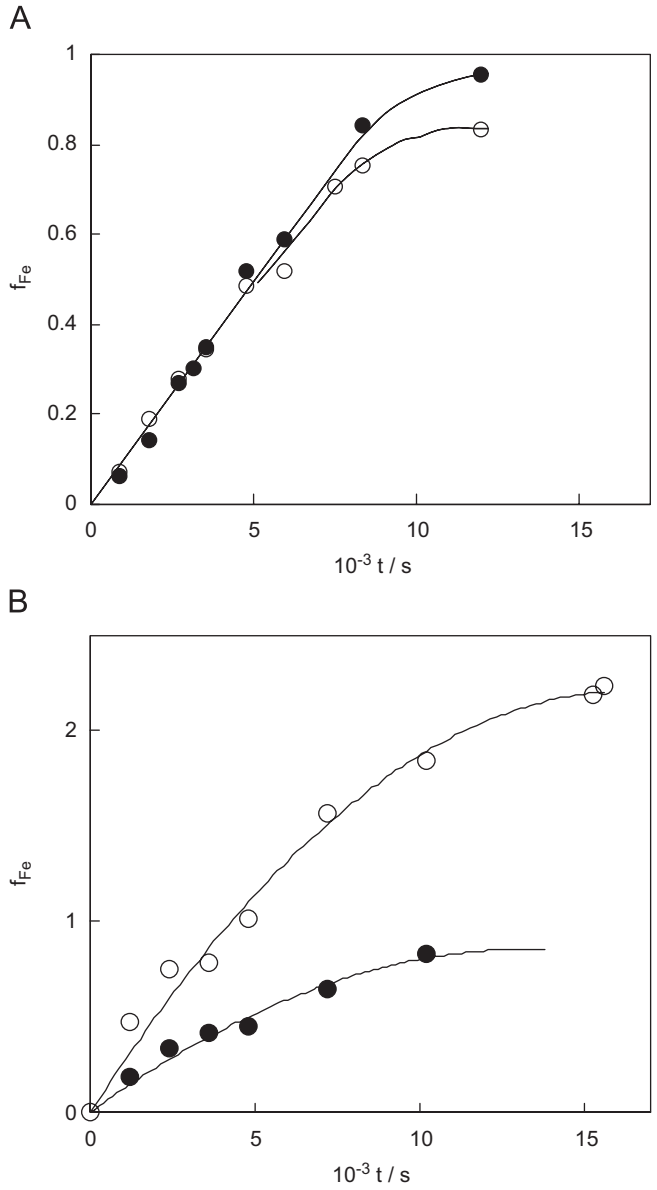

Fig. 4. Time evolution of the dissolved iron fraction in deaerated (●) and oxygen-saturated solution (○): (A) $CoFe_2O_4$; (B) $NiFe_2O_4$. Experimental conditions: 0.1 M oxalic acid at 70 °C and pH 3.5 ($I = 0.5$ M $NaClO_4$).

photochemical dissolution of Fe_2O_3 (Fig. 5). The difference is in agreement with the change in the stoichiometry, and the photochemical production of ferrous ion (see Section 4).

For ferrites, at high ferrous ion concentrations, the effect of light disappears, but the reactivity trend remains unchanged. Fig. 7 shows the dependence on $[Fe^{2+}]_o$ of the relationship $R'' = {}^{ph}k_M^{Fe(II)}/k_M^{Fe(II)}$, where $k_M^{Fe(II)}$ and ${}^{ph}k_M^{Fe(II)}$ are the thermal and photochemical specific rate constants at any given value of $[Fe^{2+}]_o$, respectively; at high concentrations the specific rates of thermal and photochemical dissolutions are equal, ${}^{ph}k_M^{Fe(II)} = k_M^{Fe(II)}$.

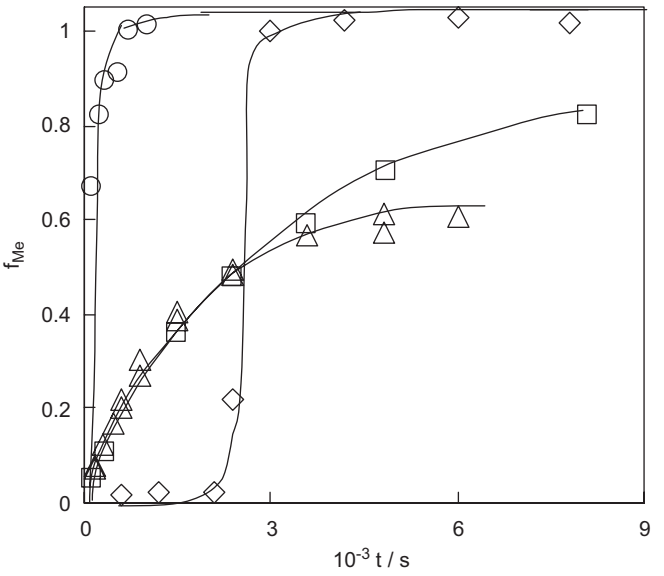

Fig. 5. Photochemical dissolution profiles for NiO (□), CoO (△), ZnO (*o*) and Fe_2O_3 (◇) in 0.1 M oxalic acid at 70 °C and pH 3.5 ($I = 0.5$ M $NaClO_4$).

Table 4
Specific photodissolution rates ${}^{ph}k_M$ (mol m^{-2} s^{-1}) for the oxides in 0.1 M oxalic acid at 70 °C and pH 3.5 and rate enhancement factors R' ($\lambda_{max} = 384$ nm, $I_o = 9.4 \times 10^{-6}$ einstein s^{-1} dm^{-3})

Oxide	$10^7 \times {}^{ph}k_M$ (mol m^{-2} s^{-1})	$R' = {}^{ph}k_M/k_M$
$Ni_{1.04}O$	0.665	1.0
$Co_{0.98}O$	77.6	1.2
$Zn_{1.02}O$	98.6	1.0
$Fe_{2.03}O_3$	–	–
$Ni_{1.15}Fe_{1.90}O_4$	0.67	18.6
$Co_{1.00}Fe_{2.00}O_4$	8.19	7.4
$Zn_{0.88}Fe_{2.08}O_4$	1.73	0.99

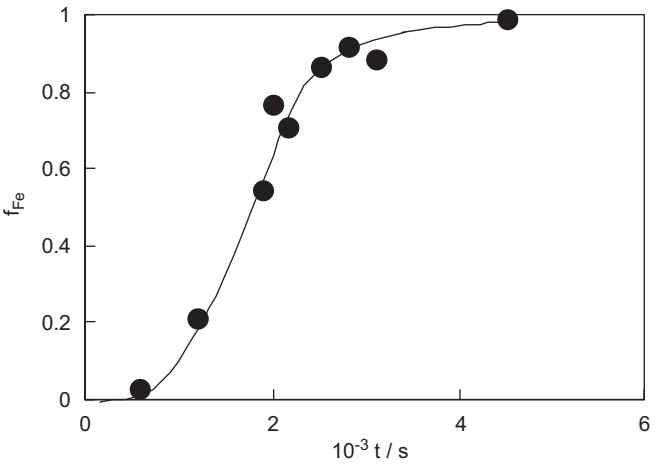

Fig. 6. Time evolution of the photodissolved fraction for $CoFe_2O_4$ at $\lambda_{max} = 384$ nm ($I_o = 9.4 \times 10^{-6}$ einstein s^{-1} dm^{-3}). Experimental conditions: 0.1 M oxalic acid at 70 °C and pH 3.5 ($I = 0.5$ M $NaClO_4$).

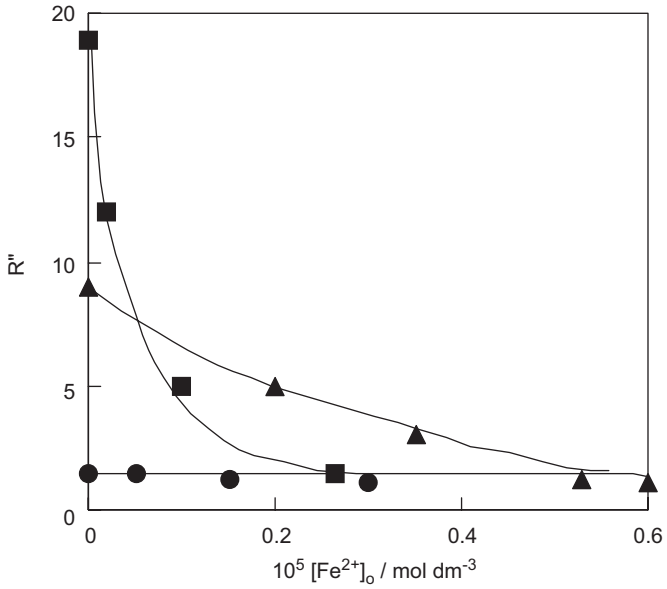

Fig. 7. Dependence on $[Fe^{2+}]_o$ of the photoacceleration factor $R'' = {}^{ph}k_M^{Fe(II)}/k_M^{Fe(II)}$ for $NiFe_2O_4$ (■), $CoFe_2O_4$ (▲) and $ZnFe_2O_4$ (●) at $\lambda_{max} = 384$ nm ($I_o = 9.4 \times 10^{-6}$ einstein s^{-1} dm^{-3}). Experimental conditions: 0.1 M oxalic acid at 70 °C and pH 3.5 ($I = 0.5$ M $NaClO_4$).

Oxygen inhibits the effect of light. In aerated media, the dissolution of all ferrites proceeds at the same rate in the dark and under light. Fig. 8 shows the coincidence of the dissolution profiles for nickel and cobalt ferrites; for comparison, the photochemical dissolution profile without oxygen is also shown.

4. Discussion

4.1. Reactivity trends in the dark

Specific rates of dissolution at any given temperature depend on solution composition. Solution pH, the nature and concentration of complexing agents, solution redox potential and ionic strength are all important. The dependence of k on solution variables has been dealt with repeatedly in the literature ([1,30,31] and references therein). In this paper, we are interested in the reactivity trends of the series of oxides under a precise set of experimental conditions. These conditions are 70 °C, 0.1 M oxalic acid, pH 3.5 and $I = 0.5$ M. The system does not contain thermally active redox reagents, although oxalate is a good reductant for Fe(III) under light. Internal redox reactions are known for both dissolved $Fe^{III}(C_2O_4)_3^{3-}$ and surface Fe^{III} oxalato complexes.

The trends in the specific dissolution rates discussed here do not apply necessarily to other experimental conditions, because of the diverse response of each system to these variables, in particular redox potential. The conditions chosen in this work are however representative of the so-called simple acid dissolution in the presence of complexing anions, or ligand-assisted acid dissolution [31–33].

The general very simplified kinetic scheme for these reactions is given in Eqs. (10) and (11), where Me = Fe or M, Ox denotes $C_2O_4^{2-}$ and the symbol ≡ identifies surface complexes. The first-order rate constant k_1 relates to the specific dissolution rate k through Eq. (12), where V is the solution volume, {≡Me–OxH} is the surface concentration (mol m^{-2}) and q is the stoichiometric coefficient for Me in $M_{1-y}Fe_{2+x}O_4$. For a detailed description of the

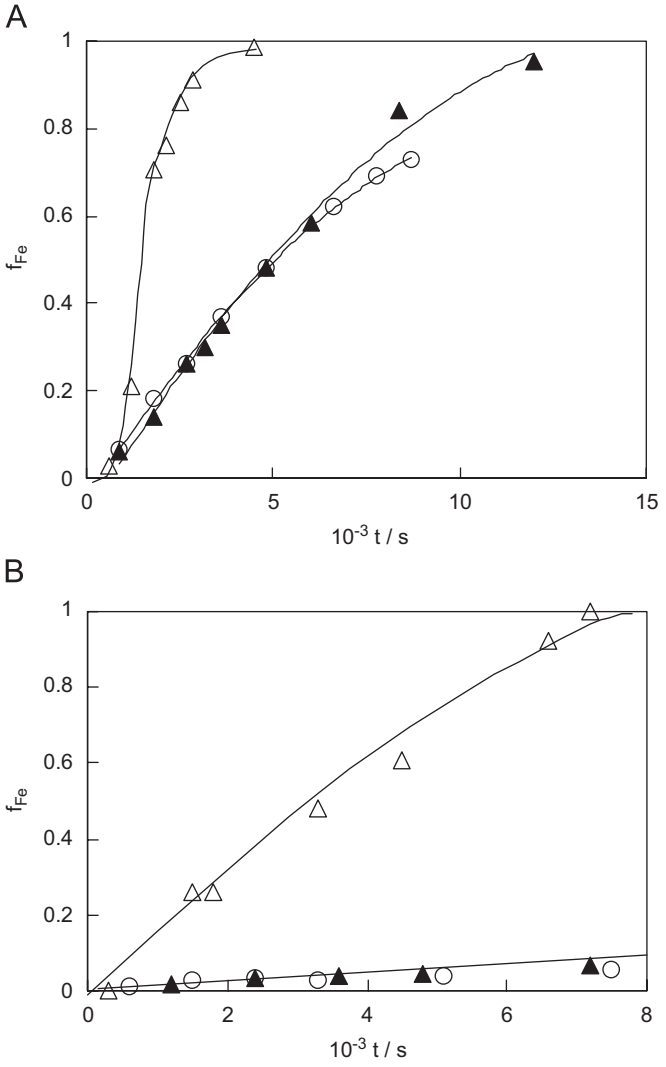

Fig. 8. Time evolution of the dissolved iron fraction in the dark (▲), under irradiation in oxygen-saturated solution (○), and under light in deaerated suspensions (△) at $\lambda_{max} = 384$ nm ($I_o = 9.4 \times 10^{-6}$ einstein s^{-1} dm^{-3}). (A) $CoFe_2O_4$; (B) $NiFe_2O_4$. Experimental conditions: 0.1 M oxalic acid at 70 °C and pH 3.5 ($I = 0.5$ M $NaClO_4$).

actual nature of surface species, see Ref. [31]:

$$\equiv MeOH + H_2Ox \leftrightarrow \equiv Me - OxH + H_2O \quad \text{fast equilibrium, } K_1 \tag{10}$$

$$\equiv Me - OxH \rightarrow Me^{n+}(aq) \quad \text{rate-determining step, } k_1 \tag{11}$$

$$(V/S)d[Me^{n+}]/dt = qk = k_1\{\equiv Me - OxH\} \tag{12}$$

Eq. (10) describes adsorption as an electroneutral reaction, although it is well known that other protolytic species of dissolved oxalate and of surface complexes may be involved [34]. When more than one surface complex may be transfered to solution, the rate law (12) involves more than one term, but this complication is not relevant for studies conducted at fixed solution composition. Eq. (11) describes the rate-determining step as the detachment of the complexed metal ion from the solid and its transfer to aqueous solution; no attempt was made to identify the speciation of the dissolved metal or to define the participation of H^+ in the stoichiometry or in the kinetics. In general, it is agreed that in acid dissolution the required number of protons equals the charge borne by the metal ion [5]. The pH dependence of the rate is embodied in k_1. In oxalic acid excess, $Me^{n+}(aq)$ is an oxalate

complex. Eqs. (10) and (11) predict that k increases with oxalate concentration, until a maximum value is reached when total coverage of surface sites is achieved ($\theta = 1$), and $\{\equiv Me\text{–}OxH\} = N_s$, the total density of surface sites. At constant oxalate and pH, a constant k value results, leading to the contracting geometry regime.

For hematite, Eqs. (10) and (11) also apply in the dark. In agreement with Siffert and Sulzberger [13], no Fe(II) is formed, despite the relatively high thermodynamic driving force, $\Delta G^0 = -0.87$ eV at pH 3 for the equilibrium represented by Eq. (8).

In terms of Eq. (12), the differences in k_1 for M and Fe are compensated by differences in $\{\equiv Me\text{–}OxH\}$. The more labile cation, with larger k_1, is therefore depleted in the surface layer. The leached layer is generated in the very early stages of dissolution ('instantaneously' in the time scale of our experiments), and must be very thin because no deviation from congruency is observed even in the earliest measurements. Such a deviation has been observed in other cases [35].

The reactivity order for mixed oxides was found to be $ZnFe_2O_4 > CoFe_2O_4 \gg NiFe_2O_4$ (see Table 2), with values of the dissolution rates lying in between those of MO and Fe_2O_3. Although the phase transfer of M(II) and Fe(III) are independent processes, the transfer of each ion exerts influence on the rate of transfer of the other. The order of reactivity is the same as that for the simple MO oxides, with lower rates defined in part (see below) by the extent of depletion of the divalent cation in the leached layer. The leached layers of the various ferrites may be viewed as a disrupted layer of the less reactive oxide, with different contents of M(II). Two factors determine the steady-state penetration rate: (a) the degree of enrichment of the leached layer in the less reactive ion, and (b) the disruption of surface layer produced by the release of the more reactive ion.

Zinc and cobalt ferrites dissolve at rates that are approximately 66 and 59 times lower than the rate of dissolution of the pure oxides ZnO and CoO, respectively, and 53 and 32 times higher, respectively, than the rate of dissolution of hematite. The leached layer may be viewed as very disrupted Fe_2O_3, causing the bulkier Zn^{2+} a larger disruption. The possible influence of the different structure of both leached layers on the effect of ferrous ion is mentioned below. The rate of hematite dissolution is only 10 times lower than that of nickel oxide; hence, the leached layer in nickel ferrite must contain appreciable amounts of both ions. The rate of dissolution of nickel ferrite is similar to that of hematite, indicating that the reactivity of surface Fe(III) is not largely affected by Ni(II). These comparisons of the rates of dissolution of pure and mixed oxides must of course be viewed with caution, because of the possible influence of particle size, shape and structure.

In a series of metal oxides undergoing acid dissolution in the presence of a complexant, it is expected that k reflects the lability of the oxo bonds linking the surface metal complex to the solid framework. In aqueous solution, a good measure of the lability of Me–O bonds is the rate of water dissociation from the coordination sphere (k_{-w}) that governs the rate of water exchange (Eq. (13)). The values of k_{-w} correlate with the rates of complexation in solution (Eigen–Wilkins mechanism [36]):

$$Me(OH_2)_m^{n+} + H_2O^* \rightarrow Me(OH_2)_{m-1}(^*OH_2)^{n+} + H_2O; \quad k_{-w} \qquad (13)$$

Table 5 shows the values of k_{-w} for Ni^{2+}, Co^{2+}, Zn^{2+} and Fe^{3+} [37], and Fig. 9 shows the plot of $\log k_{Me}$ vs. $\log k_{-w}$ for pure and mixed oxides. The data corresponding to the first fit to a linear relationship, $\log k_{Me} = -9.636 + 0.616 \log k_{-w}$, demonstrate that the lability of the oxo bonds linking the surface oxalato complex to the solid framework is determined by the intrinsic properties of Me. Basically, the (charge/radius) ratio and the crystal field effects determined by the d-electron configuration govern the rate. For

Table 5
Rate constants k_{-w} for water exchange [37]

Metal ion	k_{-w} (s^{-1})
Ni^{2+}	3×10^4
Co^{2+}	2×10^6
Zn^{2+}	7×10^7
Fe^{3+}	2×10^2

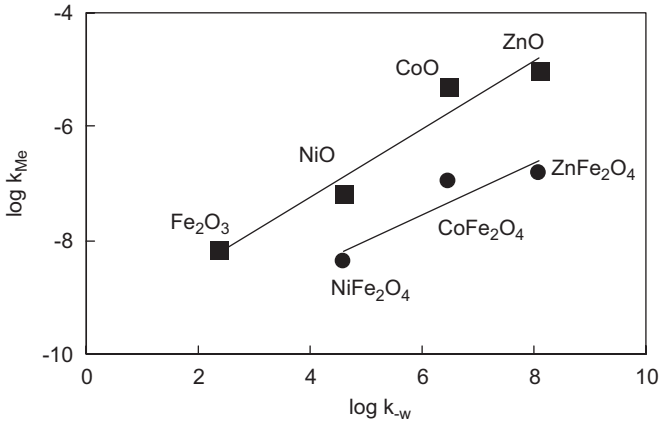

Fig. 9. Relationship between $\log k_{Me}$ and $\log k_{-w}$ for MFe_2O_4 (●) and for MO and Fe_2O_3 oxides (■).

ferrites the slope is 0.471 instead of 0.616. Thus, the dissolution of ferrites is less sensitive to the lability of M (measured by k_{-w}). The presence of Fe(III) in the solid framework not only produces an overall lowering of the line in Fig. 9. The deceleration factor (already discussed) is larger for the more labile ions, thus decreasing the slope.

Sellers and Williams [38] studied the kinetics of dissolution of four different stoichiometric spinel ferrites MFe_2O_4 (M = Fe(II), Ni, Co, Mn) in oxalic acid media under more drastic conditions, 140 °C and pH 2.5. The order of reactivity was found to be $Fe_3O_4 > MnFe_2O_4 > CoFe_2O_4 > NiFe_2O_4$. Including in our own series the value for the initial rate of magnetite dissolution [29], the order $Fe_3O_4 > ZnFe_2O_4 > CoFe_2O_4 \gg NiFe_2O_4$ is obtained. The reactivity trend is similar to ours, even though under the conditions used by Sellers and Williams, the stoichiometry of the reaction is reductive, Eq. (9), more comparable with our photochemical dissolution (see below). The position of Fe in both trends merits comment; it reflects the operation of a different mechanism. It has been amply documented that Fe(II) salts in the presence of carboxylate ligands accelerate the dissolution of Fe(III) oxides, through a mechanism involving the formation of surface mixed valence bridged dimers $\equiv Fe^{III}\text{–}L\text{–}Fe^{II}\text{–}L$ [29], which undergo internal electron exchange and produce more labile surface $\equiv Fe^{II}$ species. Note that in the systems studied by Sellers the concentration of Fe^{2+} increases as the dissolution proceeds, albeit by different mechanisms for M = Fe(II) and for $M \neq$ Fe(II).

The effect of oxygen confirms the above discussion. Iron(III) oxides dissolve faster in reductive media, whilst nickel(II) oxide dissolves faster in oxidizing media [1]. In agreement, dissolved oxygen brings about the faster dissolution of nickel ferrite, and does not affect appreciably the dissolution rates of the other two ferrites (Fig. 4). Catalysis of nickel(II) oxides dissolution by oxygen involves oxidation of surface metal centers, and enhances the transfer rate of Ni(III); the last rapidly reduces back to Ni(II) and the stoichiometry is not affected [1], except in the possible parallel oxidation of oxalate by dissolved oxygen (undetectable under our experimental conditions).

The effect of added Fe(II) on cobalt and nickel ferrites dissolution is also in line with these ideas. The rate of Fe(III) transfer is increased as discussed above, and the steady-state dissolution condition is shifted to higher rates.

In cobalt ferrite, the rate enhancement in the presence of Fe(II) is large, and the rate of dissolution becomes 41% that of pure CoO. Thus, the possibility that the composition of the leached layer is drastically altered must be considered. It has been documented previously that electron injection may be followed by electron hopping within the solid cobalt ferrite, in adjacent Fe^{III}–O–Fe^{II} moieties, which propagates appreciably in the solid; thus, a thick disrupted region may be generated [39,40]. The coordination environment of Fe^{III} in the inverse spinel is probably also important in facilitating the labilization by electron transfer.

The acceleration observed in nickel ferrite is also high, indicating not only an easy release of Fe^{III}, but also an enhancement of the transfer rate of Ni(II); this metal is transfered 1.6 times as fast as in pure NiO. As indicated above (see Fig. 3), the acceleration produced by Fe(II) at high concentrations is similar for nickel and cobalt ferrites. At lower concentrations, the pre-equilibrium of bridged dimer formation limits the observed rate enhancement. Fig. 3 shows that Fe(II) is more easily incorporated in the leached layer of nickel ferrite (larger K_L); thus, except at the highest concentration, the acceleration brought about by Fe(II) is larger in nickel ferrite.

In the case of zinc ferrite, no acceleration by Fe(II) is observed, although it has been reported that the acid dissolution of zinc ferrite is accelerated at low pH by high concentrations of Fe(II) [41,42]. It is thus possible that the lack of effect of Fe(II) under our conditions is due to very low values of K_L, rather than due to low values of $k_{M\,\max}^{Fe(II)}$. We cannot give a rationale for the order of K_L values thus derived ($NiFe_2O_4 > CoFe_2O_4 \gg ZnFe_2O_4$). The fact that zinc ferrite contains only octahedral iron whereas the other two ferrites contain part of the iron in the more labile tetrahedral environments may be relevant, regarding changes in both K_L and $k_{M\,\max}^{Fe(II)}$.

As a result of all these factors, the reactivity order at high Fe(II) concentrations is $CoFe_2O_4 \gg ZnFe_2O_4 > NiFe_2O_4$.

4.2. Reactivity trends under light

As stated, dissolution of NiO and ZnO is enhanced by oxidants [1]. However, the photogeneration of holes by light absorption does not lead to higher rates (Table 4). In the case of NiO, a p-type semiconductor, this result is expected: the concentration of holes does not change appreciably under light. On the other hand, the lack of enhancement in n-type ZnO reflects the high rate of thermal dissolution; the photochemical pathway, limited by the light intensity and the low quantum yields, does not add significantly to the overall rate [43,44].

The increased extent of p-type CoO dissolution at long times (Figs. 1 and 5) reflects changes in the precipitation of sparingly soluble $Co(C_2O_4)$. The initial photochemical and thermal rates do not differ much, and the different maximum degree of dissolution achieved in both cases must be determined by the different onset of precipitation. The rate enhancement factor quoted in Table 4 is rather imprecise, and not very different from unity.

Thus, light does not seem to affect appreciably the rates of dissolution of all three M(II) oxides. On the other hand, the influence on hematite dissolution is drastic, amply documented in the literature [7,13,45,46]. Fe(III) oxides dissolve very fast in the presence of reductants; this is specially true for magnetite dissolution in the presence of Fe(II) [47]. Surface Fe^{III} oxalato complexes are good electron acceptors, and this holds true both for external chemical reductants and for photogenerated conduction band electrons [7]. Thus, a reactive pathway opens through the generation of surface Fe^{II}. The sigmoidal profile indicates that light triggers dissolution but, more important, changes the stoichiometry of dissolution. In oxalate solution under light, all iron is rapidly converted to Fe^{II}, and a very efficient external reductant is thus generated. Eqs. (14)–(17) describe the involved chemistry.

(a) *Fast complexation*:

$$\equiv Fe^{III}OH + H_2Ox \leftrightarrow \equiv Fe^{III} - OxH + H_2O \quad (14)$$

(b) *Induction period* (*generation of dissolved Fe(II)*):
(b1) Phase transfer of Fe(III) and photochemical reduction in solution

$$\equiv Fe^{III} - OxH \rightarrow Fe(Ox)_3^{3-} \xrightarrow{h\nu} Fe(Ox)_2^{2-} \quad (15)$$

(b2) Photochemical reduction in the solid surface and phase transfer of Fe(II)

$$\equiv Fe^{III} - OxH + e_{cb}^- \rightarrow \equiv Fe^{II} - OxH^- \rightarrow Fe^{II}(Ox)_2^{2-} \quad (16)$$

(c) *Redox dissolution*:

$$\equiv Fe^{III} - OxH + Fe^{II}(Ox)_2^{2-} \leftrightarrow \equiv Fe^{III} - OxH \cdots Fe^{II}(Ox)_2^{2-} \rightarrow \equiv Fe^{II} - OxH^- \cdots Fe^{III}(Ox)_2^- \rightarrow -Fe^{II}(Ox)_2^{2-} + Fe^{III}(Ox)_3^{3-} \quad (17)$$

Concerning the ferrites, the behavior reactivity trends under light are largely similar to those in the presence of Fe(II). Thus, the reactivity order is the same (Table 4), oxygen inhibits the effect of light (Fig. 8), and light has no influence at high Fe(II) concentrations (Fig. 7). Also, light has no effect on the dissolution of zinc ferrite. All these observations signal that the main effect of light is to produce Fe(II). The slightly sigmoidal kinetic profile shown in Fig. 6 supports this interpretation. The acceleration period corresponds to the build-up of Fe(II) in solution. Inspection of the values of $R' = {}^{ph}k_M/k_M$ for nickel and cobalt ferrites (Table 4) also agrees with this idea. The larger K_L values for nickel ferrite render low levels of photolytic Fe(II) adequate to produce a large enhancement. The slightly sigmoidal profile in the photochemical dissolution of cobalt ferrite (Fig. 6), not observed in nickel ferrite, can also be explained in terms of the respective K_L values.

Fe(II) can be generated directly in the oxide surface, if the solid absorbs the radiation, or can be generated by photolysis of dissolved trisoxalatoferrate(III) [48]. The prevalence of either possibility depends on the light fraction absorbed by the solid and by the dissolved species. In the very initial stages, light is absorbed essentially by the solid, but Fig. 6 shows that there is no clear evidence of acceleration of the initial rate. Once appreciable values of dissolved iron fraction are reached, solution photolysis dominates the process.

Photochemical dissolution of iron oxides is considered an important mechanism of iron mobilization in aquatic media. Direct irradiation in water does indeed generate electron–hole pairs, the former being able to promote iron phase transfer, in the form of Fe(II). This process however requires the presence of a hole scavenger, oxalic acid in our case, natural organic matter in aquatic environments. In the presence of hole scavenger, the alternative of solution photolysis becomes possible, and it is not possible to demonstrate unambiguously if direct oxide photolysis is involved, or if solution photolysis alone suffices to account for the observations. It has been proposed that photochemical dissolution of metal oxides is defined by the availability of minority carriers (electrons for p-semiconductors, and holes for n-semiconductors) [49]. Because of the effects described in this paper, it is difficult to test this hypothesis. No correlation exists between the dissolution behavior of $NiFe_2O_4$ (p-type) and $CoFe_2O_4$ (n-type) and the nature of the minority carriers.

5. Conclusions

The dissolution rates of pure oxides correlate with the rates of water substitution in aqueous Me^{n+}. Also, light accelerates dissolution when electron trapping by the surface complexes originates a new, efficient dissolution pathway. This is true even for an n-type semiconductor as hematite. No observable effect is found for oxides prone to oxidative dissolution. Trapping of electrons, intrinsically less reactive than holes, is responsible for important photodissolution. However, even in this case, light only triggers the onset of a thermal dissolution pathway involving dissolved Fe(II).

Nickel ferrite dissolution is accelerated by both reductants (Fe^{2+}) and oxidants (O_2), demonstrating that the dissolving interface contains appreciable amounts of both Ni(II) and Fe(III).

Dissolution of zinc and cobalt ferrites on the other hand is only accelerated by reductants, because the leached layer contains low concentrations of the divalent cation.

There is a linear relationship between k_{Me} and k_{-w} for simple oxides, and, although somewhat blurred, for spinel ferrites. The lability of the metal ion governs the rate of dissolution. Fe(III) arrests more the reactivity of the more labile ions, thus producing a lower slope and a worse linear correlation. Photochemical dissolution is important in Co and Ni ferrites, whereas it is ineffective for CoO, NiO and ZnO. More important than the generation of electron/hole pairs in the oxide, the well-known photochemistry of Fe(III) in oxalic media seems to account for the results.

Acknowledgments

This work was carried out with Grants from ANPCyT (PICT 13534), CONICET (PIP 5978) and CNEA (Program P5), and was part of the LAGR Ph.D. Thesis.

References

[1] M.A. Blesa, P.J. Morando, A.E. Regazzoni, Chemical Dissolution of Metal Oxides, CRC Press, Boca Raton, FL, 1994.
[2] D.A. Dzombak, F.M.M. Morel, Surface Complexation Modeling: Hydrous Ferric Oxide, Wiley-Interscience, New York, 1990.
[3] A.D. Weisz, Ph.D. Thesis, Universidad de Buenos Aires, 2001.
[4] C. Ludwig, W.H. Casey, P.A. Rock, Nature 375 (1995) 44.
[5] C. Ludwig, W.H. Cassey, J. Colloid Interface Sci. 178 (1996) 176.
[6] D. Suter, S. Banwart, W. Stumm, Langmuir 7 (1991) 809.
[7] B. Wehrli, B. Sulzberger, W. Stumm, Chem. Geol. 78 (1989) 167.
[8] S. Banwart, S. Davies, W. Stumm, Colloids Surf. 39 (1989) 303.
[9] Y. Zhang, N. Kallay, E. Matijević, Langmuir 1 (1985) 201.
[10] C.A. Figueroa, E.E. Sileo, P.J. Morando, M.A. Blesa, J. Colloid Interface Sci. 225 (2000) 403.
[11] T.D. Waite, F.M.M. Morel, J. Colloid Interface Sci. 102 (1984) 121.
[12] T.D. Waite, F.M.M. Morel, Environ. Sci. Tech. 18 (1984) 680.
[13] C. Siffert, B. Sulzberger, Langmuir 7 (1991) 1627.
[14] M.I. Litter, M.A. Blesa, J. Colloid Interface Sci. 125 (2) (1988) 679.
[15] M.I. Litter, M.A. Blesa, Can. J. Chem. 70 (1992) 2502.
[16] B. Arnison, R. Segall, R. St.C. Smart, P.S. Turner, J.Chem. Soc. Faraday Trans. 1 (77) (1981) 535.
[17] N. Sato, Electrochemistry at Metal and Semiconductor Electrodes, Elsevier, 1998.
[18] H. Tamura, E. Matijević, J. Colloid Interface Sci. 90 (1981) 100.
[19] U. Schwertmann, R.M. Cornell, Iron Oxides in the Laboratory, VCH, Weinheim, 1991.
[20] D.L. Leussing, N. Newman, J. Am. Chem. Soc. 78 (1956) 552.
[21] Data Base from International Center for Diffraction Data (ICDD), PDF 22-1189.
[22] Data Base from International Center for Diffraction Data (ICDD), PDF 42-1300.
[23] Data Base from International Center for Diffraction Data (ICDD), PDF 36-1451.
[24] Data Base from International Center for Diffraction Data (ICDD), PDF 33-0664.
[25] Data Base from International Center for Diffraction Data (ICDD), PDF 10-0325.
[26] Data Base from International Center for Diffraction Data (ICDD), PDF 22-1086.
[27] Data Base from International Center for Diffraction Data (ICDD), PDF 22-1012.
[28] C.G. Hatchard, C.A. Parker, Proc. R. Soc. A 235 (1956) 518.
[29] M.A. Blesa, H.A. Marinovich, E.C. Baumgartner, A.J.G. Maroto, Inorg. Chem. 26 (1987) 3713.
[30] G. Furrer, W. Stumm, Chimia 37 (1983) 338.
[31] M.A. Blesa, A.D. Weisz, P.J. Morando, J.A. Salfity, G.E. Magaz, A.E. Regazzoni, Coord. Chem. Rev. 196 (2000) 31.
[32] B. Zinder, G. Furrer, W. Stumm, Geochim. Cosmochim. Acta 50 (1986) 1861.
[33] E. Wieland, B. Wherli, W. Stumm, Geochim. Cosmochim. Acta 52 (1988) 1969.
[34] C.A. Figueroa, E.E. Sileo, P.J. Morando, M.A. Blesa, J. Colloid Interface Sci. 244 (2001) 353.
[35] S. Jacobo, A.E. Regazzoni, M.A. Blesa, J. Mater. Sci. 37 (2002) 3053.
[36] M. Eigen, R.G. Wilkins, Adv. Chem. Ser. 49 (1965) 55.
[37] F.M.M. Morel, J.G. Hering, Principles and Applications of Aquatic Chemistry, Wiley-Interscience, New York, 1993.
[38] R.M. Sellers, W.J. Williams, Faraday Discuss. Chem. Soc. 77 (1984) 265.
[39] M.A. Blesa, A.J.G. Maroto, P.J. Morando, J. Chem. Soc. Faraday Trans. I 82 (1986) 2345.
[40] E.E. Sileo, L. García Rodenas, C.O. Paiva-Santos, P.W. Stephens, P.J. Morando, M.A. Blesa, J. Solid State Chem. 179 (2006) 2237.
[41] K. Nii, Y Hisamatsu, Trans. NRIM 8 (5) (1966) 27.
[42] F. Elgersema, G.F. Kamst, G.J. Witkamp, G.M. van Rosmalen, Hydrometallurgy 29 (1992) 173.
[43] J. Doménech, A. Prieto, J. Phys. Chem. 90 (1986) 1123.
[44] G. Rogers, G. Simkovich, K. Osseo-Asare, Hydrometallurgy 10 (1983) 313.
[45] T.D. Waite, A. Torikov, J.D. Smith, J. Colloid Interface Sci. 112 (1986) 412.
[46] N.N. Kalyazin, A.F. Nechaev, Russ. J. Phys. Chem. 58 (1984) 693.
[47] E.C. Baumgartner, M.A. Blesa, H.A. Marinovich, A.J.G. Maroto, Inorg. Chem. 22 (1983) 2224.
[48] M.I. Litter, E.C. Baumgartner, G.A. Urrutia, M.A. Blesa, Environ. Sci. Technol. 25 (11) (1991) 1907.
[49] V.A. Myamlin, Y.V. Pleskov, Electrochemistry of Semiconductors, Plenum Press, New York, 1967.